International Journal of Engineering Trends and Technology
ISSN: 2231–5381 / https://doi.org/10.14445/22315381/IJETT-V71I4P228

Volume 71 Issue 4, 323-331, April 2023

Original Article

Mechanical and Electromagnetic Shielding Properties of TIG Welded Dissimilar Aluminum Alloys

Veeraiah Goriparthi[1,2*], Ramanaiah Nallu[2], Sudhakar I[1], BVSRN Santhosi[3]

[1]*Department of Mechanical Engineering, MVGR College of Engineering (A), Vizianagaram, India*
[2]*Department of Mechanical Engineering, AU College of Engineering, Andhra University, Visakhapatnam, India*
[3]*Department of Physics, MVGR College of Engineering (A), Vizianagaram, India*

[*]*Corresponding Author : veeraiah@mvgrce.edu.in*

Received: 01 March 2023 Revised: 10 April 2023 Accepted: 17 April 2023 Published: 25 April 2023

Abstract *- In present days, defence sectors like shipbuilding and aerospace are facing hurdles in developing EM (electromagnetic) wave-absorbing materials. Researchers and scientists focused on developing materials like glass fibre composites, polymer composites and, to some extent, metal matrix composites for the mentioned applications. Polymer-based composites show relatively good shielding against EM waves with the cost of mechanical properties. Metal matrix composites (MMC) in specific aluminium offer high mechanical strength and moderate shielding effectiveness compared to fibre and polymer composites. To use these in intended applications joining is required at some sort of time. The joining technique significantly influences the joint properties and further affects the performance. Researchers mainly focused on developing EM wave materials than focusing on the effect of the joining technique on the mechanical and EM properties of the developed material. In the present work, an attempt has been made to study the effect of the joining technique on the mechanical and EM wave properties of dissimilar aluminium alloys.*

Keywords *- TIG welding, Dissimilar aluminium alloys, Tensile strength, Micro-vicker hardness, Pitting corrosion, EM wave properties.*

1. Introduction

In a hostile environment, warships and fighter jets should escape from EM signals generated by the RADAR of the opponent. The mission success rate directly depends on the detectability of the opponent's RADAR signals. Radar cross-section reduction (RCS) measures fighter jet or ship detectability to opponent RADAR signals. RCS reduction could be possible with shape optimization using advanced EM wave-absorbing materials. However, shape optimization could affect aerodynamic performance [1-5]. Developing EM wave-absorbing materials like polymer and fibre-based composites and MMC can mitigate these problems. The main drawback of polymer-based composites is low strength and poor resistance against environmental conditions compared to metal alloys and MMC [29]. Also, continuous maintenance and not being apt for load-bearing structures make them unsuitable for the mentioned applications. EM wave attenuation with excellent mechanical properties needs to be addressed by microwave engineers and material scientists working on developing advanced equipment for stealth and defence sectors [1-3]. With the successful advancement of the aerospace and shipbuilding age, massive electronic equipment (such as high-power radars, inertial navigation systems, communication stations, and onboard computers) has evolved into a vital component of aircraft with various purposes. This wirelessly operated electronic equipment will produce unwanted Electromagnetic (EM) radiation, which will disrupt the biological environment of the pilots as well as the nearby electronic equipment's ability to operate normally. For non-planar sections like the skin, hatch cover, and other electrical equipment, strong Electromagnetic Interference (EMI) shielding performance materials are required. Utilizing flexible EMI shielding materials with high EMI Shielding Effectiveness (SE) is much sought after in these situations to solve EMI issues. Nowadays, due to their affordability, most researchers use synthetic polymer textiles or cellulose-based fabrics as their supporting substrates. However, in particular applications like aerospace and shipbuilding, the mechanical strength of EMI shielding materials plays an important role. The aforementioned materials act as a good shield against EM waves with the cost of mechanical strength. To mitigate these problems, researchers are focusing on lightweight materials like aluminium and its composites as EM shield materials as they compete with steels in terms of mechanical properties and offer (aluminium composites) reasonably good shielding efficiency. Many investigators studied the performance of EM wave absorbing materials in X-band (8.2-12.4 GHz) frequency. The production of shielding material using aluminium composites, specifically aluminium 2024 combined with CFA and aluminium 2024 combined with

PFA, was reported by Dou et al. [7]. These alloys provided excellent shielding effectiveness up to 100.0 MHz but began to degrade at 600 MHz and further degraded exponentially at 1.0 GHz in comparison to 2024 Al. Thus, it was concluded that at 1.0 GHz, 2024 aluminium provided substantially superior shielding than CFA/2024 Al. A new sandwich composite made of ferro-aluminum for shielding magnetic and electromagnetic interference was created by hot pressing and subsequent diffusion treatment. Sandwich composite's electromagnetic shielding efficiency is greater than that of a pure iron plate. It rises with the extension of the diffusion period, reaching 70 to 80 dB at frequencies between 30 KHz and 1.5 GHz. The key factor improving the shielding performance of the sandwich composite is the multiple reflection loss in the Fe-Al gradient layer[8]. In the frequency range of 30.0 kHz-1.5 GHz, the electromagnetic interference shielding effectiveness (EMSE) characteristics of the composites were evaluated. The findings showed that the two different types of composites' EMSE characteristics were largely equivalent. In the frequency ranges of 30.0 kHz–600.0 MHz, adding fly ash particles enhanced the shielding efficiency attributes of the matrix aluminium, and the increment varied with increasing frequency [9]. The shielding efficiency of aluminium 6061 composites reinforced with al2o3, SiC and fly ash has been significantly affected. Composites fabricated with 10 weight percent each of Al2O3 and SiC and 5 weight percent of fly ash showed excellent mechanical and EM shielding properties [10]. Similar observations were found in another study on Al6061 composites reinforced with the aforementioned elements [11].According to Yao et al. [12], the addition of nickel fibre greatly reduces the electromagnetic shielding performance of materials made of cement. The SE of the nanocomposites with cement as the foundation directly increases with an increase in the nickel fibre content. The highest reported shielding efficacy for a doped nickel fibre composite was 24.48 dB at 120 MHz. Researchers successfully developed the EM shielding materials with aluminium alloy and composites despite joining difficulties. The usage of aluminium alloys and composites is limited in specific applications due to poor joining abilities. in the present study effect of the joining technique on mechanical and EM properties of two aluminium alloys AA5083-O and AA7075-T651. The TIG welding technique joins the two base alloys, and the effect of the welding technique on weld joints in terms of mechanical and EM shielding properties has been investigated. Many researchers investigated the effect of the TIG welding technique on the mechanical properties of aluminium alloys. The joining of AA5083 aluminium alloy was tested using TIG welding with the aim of finding the best processing parameters, such as weld current and gas flow rate, for improved weld strength. It was discovered that high heat input, or high current, was not ideal for joining aluminium alloys [30].A comparison of welding AA 6061 aluminium alloy utilising cold metal transfer (CMT), TIG, and TIG-CMT hybrid techniques showed that the hybrid joint's weld penetration was deeper than the combined depth of the penetrations of the TIG joint and the CMT junction[14-15]. Both GMAW and GTAW were successfully used to fabricate aluminium alloy weldments, with GTAW weldments having superior mechanical qualities over GMAW weldments [16]. Defect-free joints were achieved during TIG welding of AA5456 with argon as shielding gas. Peak current, base current, welding speed, and pulse frequency influenced the production of a fine, equiaxed grain structure in the weld zone during pulse TIG welding of aluminium alloy AA5456[17]. The authors found that researchers focused on the characterization of aluminium alloy and MMC in terms of mechanical and electrical parameters. Further, aluminium alloys successfully joined through the TIG welding technique. To the best of the author's knowledge, the effect of the TIG welding technique on the mechanical and EM properties of aluminium alloy is not found in the open literature.

2. Materials and Methods

The two aluminium alloys AA7075-T651 and AA5083-O used in the present investigation were received in rolled condition. Chemical composition of alloys found by spectroscope (Make: Shimadzu Analytical) and presented in table-1. Mg-rich (ER 5083) aluminium was chosen as filler material for the present study.

2.1. TIG Welding and Samples for Characterization

Gas Tungsten Arc Welding (GTAW/TIG) was used to create square butt dissimilar weld joints using previously chosen AA7075-T651 and AA5083-O aluminium sheets (with dimensions of 100 mm x 100x mm3 mm). Weld process parameters were considered as weld current in the 80 amp - 120 amp range, argon as a shielding gas with 15 L/min maintained during the welding process. Cross sections samples sliced from fabricated weld joints for characterization of Microstructure and SEM analysis. Sliced specimens were polished using a belt grinding machine, and Keller's reagent (95% H_2O, 2.5% HNO_3, 1.5% HCl, and 1% HF) was used to reveal microstructural features. SEM with EDAX (LEO 440UK make) was used to characterize the weld zone of fabricated weld joints.

Table 1. Chemical composition of base materials

Alloy	Element (in wt. %)								
	Si	Fe	Cu	Mn	Mg	Cr	Zn	Ti	Al
AA7075-T651	0.04	0.15	1.30	0.02	2.30	0.19	5.40	0.05	90.55
AA5083-O	0.09	0.27	0.01	0.80	4.40	0.07	0.02	0.02	94.32

Vickers's micro hardness test machine Model: VH1202, Buehler, the USA, make used to measure the hardness across the transverse direction of welding. Tensile samples cut along the transverse direction of the weld line and tensile strength of weld joints were obtained using a universal testing machine (Model:5582, Instron, UK) with a strain rate 0.001mms^{-1}

A software-based Gill AC electrochemical system is used to conduct potentio dynamic polarization tests to study the pitting corrosion behavior as per ASTM G106 standard. All experiments were conducted in aerated 3.5%NaCl solutions with pH adjusted to 10 by adding potassium hydroxide. The potential scan was carried out at 0.166 mVs-1 with the initial potential of –0.25V (OC) SCE to the final pitting potential. All the fabricated weld joints characterized for EM wave properties like permeability, permittivity, conductivity and shielding effectiveness in X-band frequency (8.2-12.4 GHz) using a vector network analyzer (Rhodes & Schwarz model ZVB 20) through waveguide technique.

3. Results and Discussion

3.1. Microstructural Examination of Weld Joints

Microstructural analysis of weld joints provides detailed information about tensile strength and hardness distribution. The joint strength is significantly influenced by the weld width and penetration—fusion zone microstructural analysis carried out for the samples fabricated at low, medium and high weld currents. The Microstructure of the TIG joint is characterized by three zones, namely, fusion zone (FZ), partially melted zone (PMZ) and heat affected zone (HAZ). The PMZ is also known as the dissolution zone, and the HAZ is termed an over-aging zone [13-15]. Heat input influenced the grain size in the dissolution zone close to the fusion line. It is observed that joints fabricated at low heat input, i.e. low weld current resulted in fine grains compared to the joints fabricated at relatively high current. It could be attributed to the high cooling rate induced at high welding current results in aging and some solution treatment after welding. In addition, high temperature over aging and coarsening of precipitates in PMZ causes an increase in the post-weld hardness of PMZ.

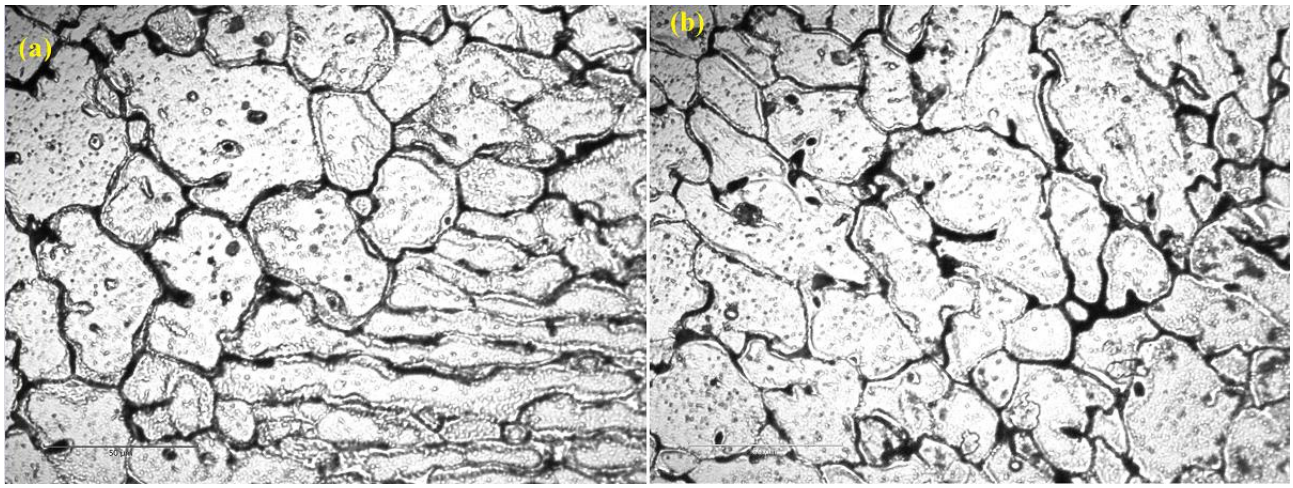

Fig. 1 (a) PMZ and FZ interface on AA7075 side (b) Fusion zone of weld joint at 100 amp

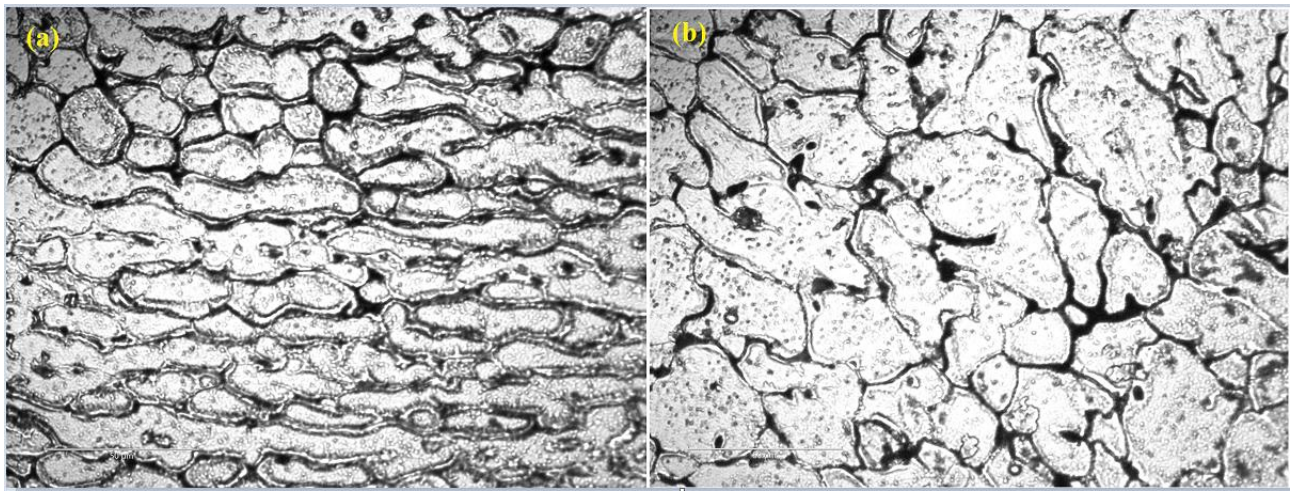

Fig. 2 (a) PMZ and FZ interface on AA5083 side (b) Fusion zone of weld joint at 100 amp

Further, high weld current (high heat input) resulted in a smoother transition between base alloys and HAZ, whereas a distinct boundary between FZ and PMZ corresponds to low heat input. The cooling rate significantly influenced the precipitate formation; higher cooling rates ensured the dendrite formation, whereas slow cooling did not enhance. Weld joint fabricated at 100 amp current has been extensively analysed for microstructural and secondary phase observation in fusion zones [26].

Weld heat input is relatively medium compared to the joints made at other currents, causing moderately fine grains in the fusion zone. As the filler used in the present investigation belongs to the AA5xxxx family, it causes solid solution formation with alloying elements like silicon [27-28]. However, Mg content reaches more than its solubility level (15 % solubility at 450° C), which causes the formation of new phases at grain boundaries or within the grains. When the weld current increases, then the solubility of Mg raises and accelerates the new phase formations [26]. In the present study, one of the base alloys corresponds to the filler wire group, so the chances for the formation of new phases are very high. Even if the Mg content is within the solubility limit, most are in the dissolved stage and form a single phase with the substrate. Fig 1 & 2 depicts the fusion zone and PMZ towards AA5083- O and AA7075 side of the weld joint fabricated at 100 amp current. As the increase in weld current raises the heat generation and promotes non-equilibrium conditions. Further, it accelerates the formation of secondary compounds like Mg_2Si, $Al_{12}(Fe\ Mn)_3Si$, Al_6 (Mn-Fe-Cr) and Al-Mg-Si intermetallic compounds [24,32].

3.2. SEM Analysis Across the Weld Zone

The microstructural detail explained earlier is further supported by SEM micrographs presented in Fig1 & 2. The weld zone consists of equiaxed grains, which are attributed to attaining high strength in weldment (fabricated 100amp). Similarly, interface characterization across both sides of weldment reveals a greater extent of disperoids dissolution along AA5083 aluminium alloy compared to AA 7075 aluminium alloy [26]. Fig.3 depicts SEM-EDAX maps of the weld joint showing the presence of major alloying elements like zinc, magnesium and copper.

Further SEM examination of micrographs reveals the presence of intermetallics and weld defects like pore formation.

Pore formation could be due to the trapping of dissolved gases into the molten weld pool during the solidification, thus resulting in bobble formation in the solidified weld. Hydrogen absorption rate increases with the rise in weld current. Weld joints fabricated at 100 amp resulted in superior mechanical properties compared to the other fabricated joints. This is attributed to relatively low porosity and the presence of strengthened intermetallics compared to the joints fabricated at other weld currents.Fig.4 (b) shows the clear formation of pores in weld joints made at high weld current, i.e. 120 amp.

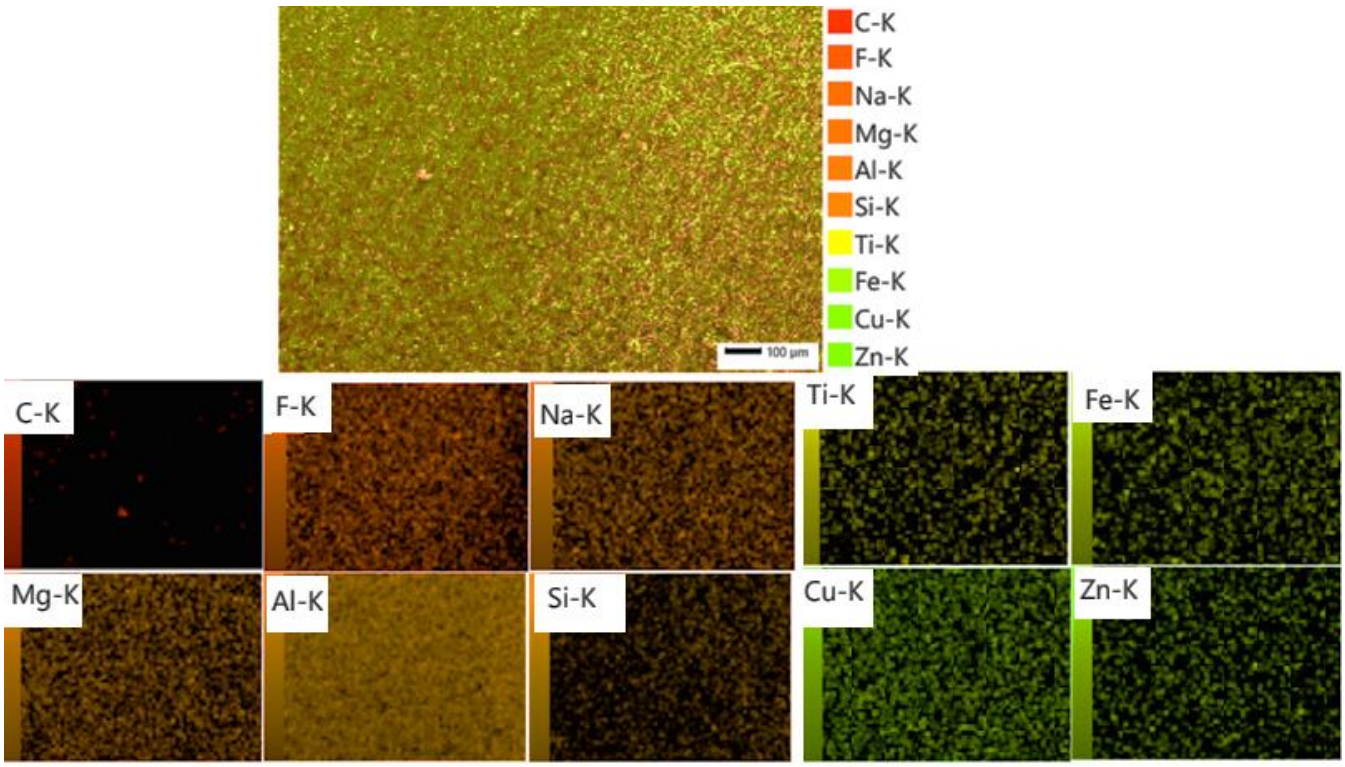

Fig. 3 SEM-EDAX maps weld joint fabricated at 100 amp

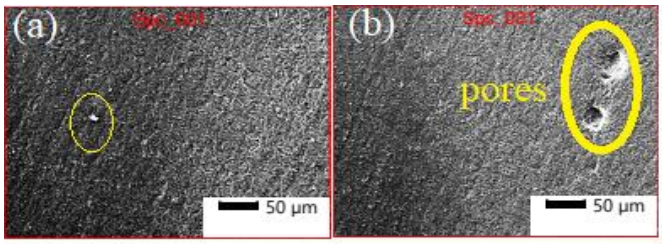

Fig. 4 SEM micrograph of weldments made (a) 100 amp (b) 120 amp

3.3. Micro-Hardness

Microhardness distribution along the transverse direction of weldments is carried out to understand joint line strength better.

Fig.5 shows the joint line hardness of all weld joints. Hardness at the joint line was found to be 138 Hv, corresponding to a 120 amp weld current. In addition, due to COVID-19 non-availability of characterization of facilities forces the natural aging for a period of 150 days since weldments are fabricated. This could also be one reason for variation in hardness distribution across the weld sections.

Earlier studies on the effect of natural aging on the mechanical properties of AA5086 and AA6061 dissimilar weld joints concluded that natural aging for a period of 70 days significantly affected the weldment mechanical properties. The hardness distribution across the weldments is significantly influenced by the liquid and solidus temperatures of the base alloy and natural aging phenomena. The FZ hardness range of all the weld joints is higher than alloy AA5083 and lower than alloy AA7075. However, the hardness towards the AA7075 alloy side is higher than the hardness of the AA5083 side. The rich Mg content of filler wire AA5356, base metal alloying elements, and prior formation of the partially melted zone (PMZ) due to low solidus temperatures could be the reasons for higher hardness towards the AA7075 side [26].

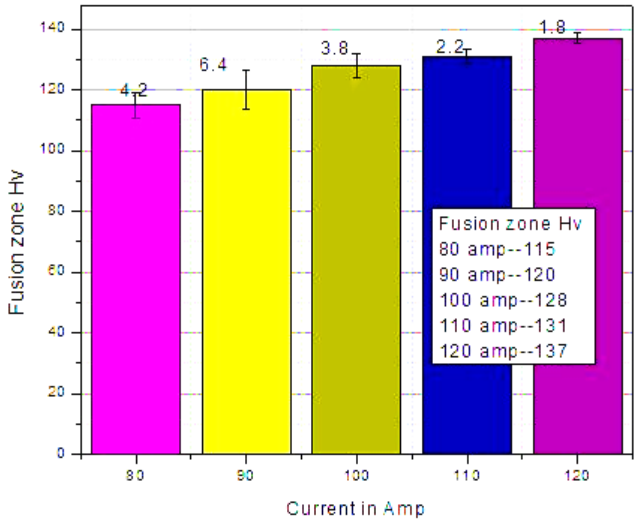

Fig. 5 Fusion zone hardness of weld joints

3.4. Tensile Test

All the stress-strain diagrams exhibited similar types of profiles. From fig. 6, the ultimate strength varies in the range of 200 MPa - 283 MPa during welding of AA5083 aluminium alloy with AA 7075 aluminium alloy and maximum weld strength is found to be 283 MPa at weld current 100 amp. From the stress and strain plot, it has been observed that the area under the stress-strain curve is minimum for a welding current of 120 Amps, while the area enclosing the same for 100 Amps is found to be maximum. It can be understood that the weld made of 120 Amps absorbs low energy before undergoing failure/ fracture, indicating the weldment's brittle behaviour. It may be due to the formation of brittle phases (which can be understood through SEM EDAX/ XRD analysis) formed during welding at the high current of 120 amp. Mode of fracture can be observed through exhaustive SEM analysis of failed samples of the weldment. The presence of intermetallic phases such as Al (Mg-Si), $MgZn_2$, Mg_2Si, Al_3Fe, Al_2Cu_2Fe, M_gAl (Cu), Al_2CuMg, Al_2CuFe_4 and other inter-metallic may be contributors to obtain weld strength [27-28].

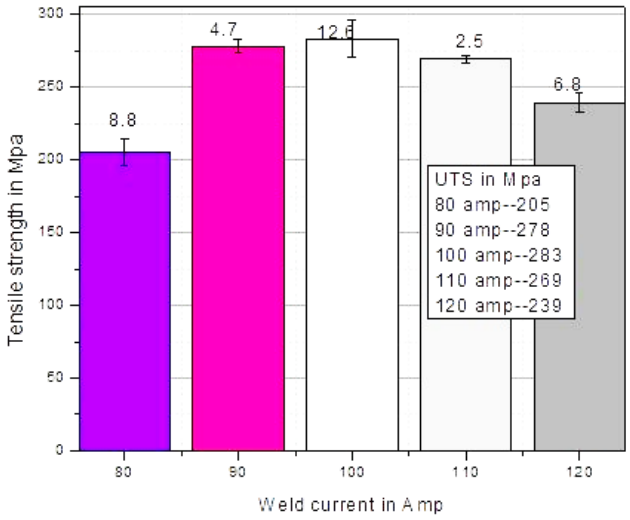

Fig. 6 Weld joint tensile strength

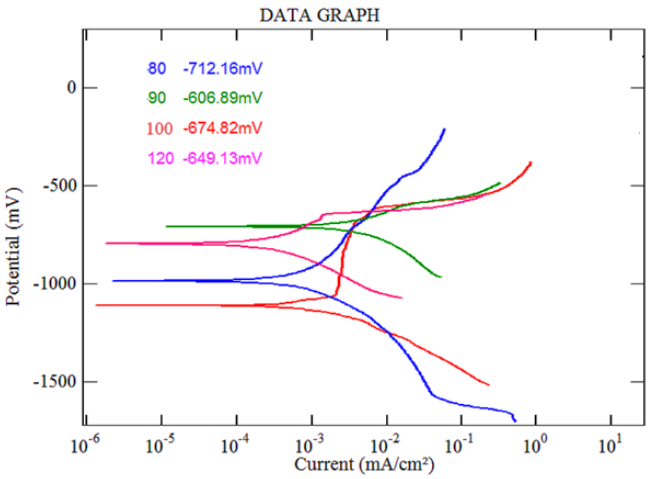

Fig. 7 Potentiodynamic polarization curves of the weld joints

3.5. Pitting Corrosion

Corrosion is known to degrade or destroy a material's functional properties and causes it to be unsuitable for the intended application. In the case of weld joints made with dissimilar materials and exposed to the external environment are prone to corrosion severely [21-22]. The addition of alloying elements significantly affects the mechanical properties and corrosion resistance of aluminium.

Elements like copper, silicon, and magnesium increase the corrosion potential, whereas the addition increases the resistance against corrosion. However, at particular temperatures and concentrations, the alloying elements do have a restricted degree of solid solubility in aluminium. When their limiting solid solubility is reached, the influence of alloying elements on the behaviour of aluminium corrosion might be deleterious. On cooling, they typically form relatively coarse component anodic and cathodic intermetallic particles, which have been proven to cause pitting as a result of the differential in corrosion potential with the surrounding aluminium matrix. This further causes the weakening of the bond between the matrix and secondary phases. Results of potentiodynamic polarization are shown in fig.7, and it can be seen that the corrosion potential (Ecorr) differs from one weld sample to another. 80 amps offer less corrosion resistance compared to others. It may be due to galvanic coupling formation between Al- matrix and intermetallic and dissolution of strengthening phases. The presence of coarse grain favours intergranular corrosion resistance (-606.89mVs) compared to fine equiaxed (-712mVs) one. The distribution of fine precipitates not only offers high strength but also may promote galvanic coupling by reducing the corrosion resistance compared to 90 amps. Thus, it is recommended to use a current of 90 amps for high corrosion resistance of welded joints, while high strength of welded joints can be attained by using 100 amps.

3.6. EM Shielding Characteristics

EMI shielding performance of base alloys' and weld joints' is assessed by using a two-port vector network analyser. The electromagnetic signal that is impinging on the surface is often oblique. However, because of the VNA via waveguide technique limits, the incidence angle examined in the current study is 90°. The Waveguide technique is first used to assess the permittivity and permeability of base alloys and weld joints. The EMI SE of the two basic alloys and the fabricated weld joints are measured based on EM wave theory. The following equation is used to compute the electromagnetic shielding effectiveness (Reflection power, Absorption power, and Transmission power) in terms of S parameters [20,23,31].

$$SE_T = 10 \log 10\frac{1}{T} = 10 \log 10\frac{1}{|S12|2} = 10 \log 10 \frac{1}{|S21|2}$$

The electric field has two different types of currents (conduction and displacement) when an EMI occurs on a metallic surface. Both the displacement current and the conductance current make up a real and an imagined portion of permittivity. Fig.8 & 9 Shown are the real and fictitious components of the complex permittivity and permeability of weld joints made with various weld currents. According to Fig.8, weld joints' permittivity's nearly constant regardless of frequency and rise as weld current increases. It is seen as a result of the conductive network rapidly building up and developing pores with rising weld currents. When EM radiation strikes metallic surfaces, the electric field causes two different types of electrical currents to flow through the material [18]. They are the displacement current caused by bound charges and the conduction current that results from the existence of free electrons in the metal [2]. The displacement current will contribute to the real portion of the permittivity, whereas the conduction current will contribute to the imaginary component of the permittivity (dielectric loss).

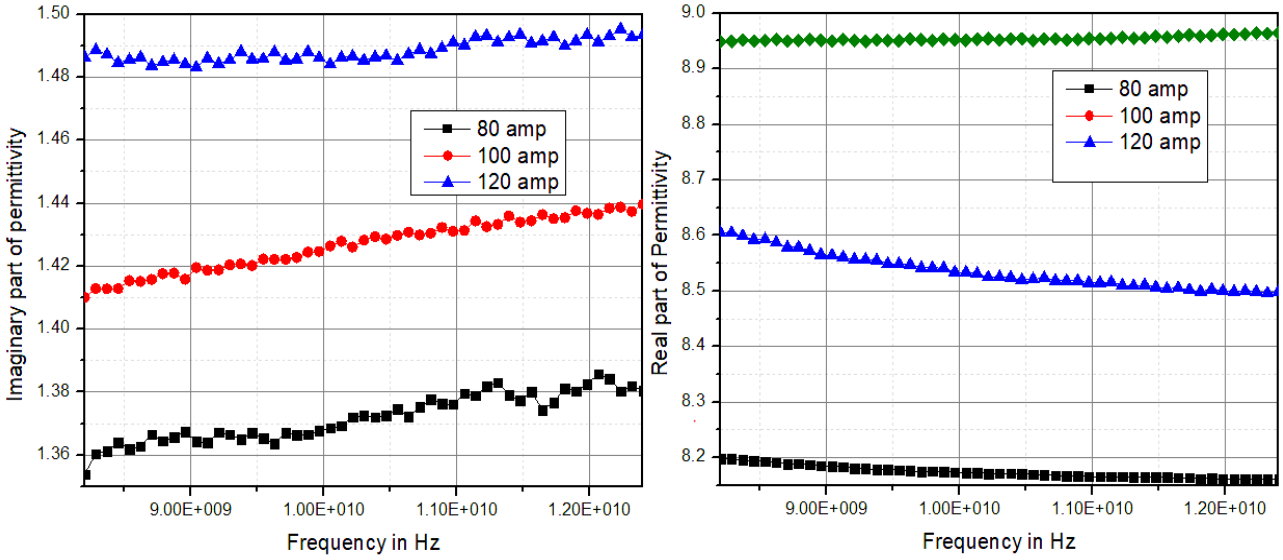

Fig. 8 Complex permittivity of TIG weld joints (a) Imaginary component (b) Real component

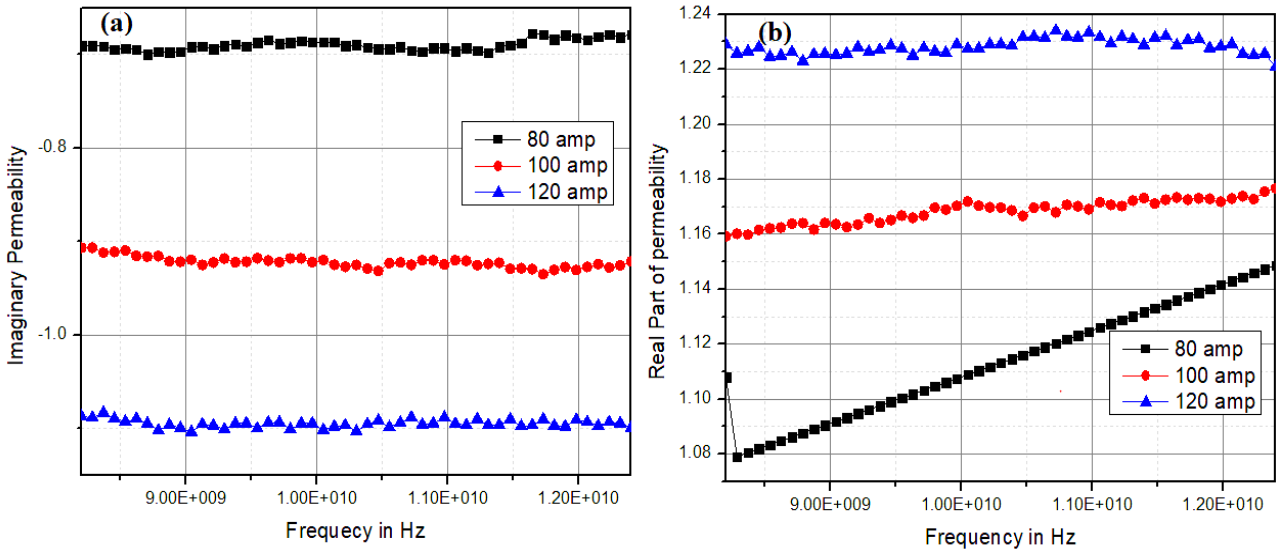

Fig. 9 Complex permeability of TIG weld joints (a) Imaginary component (b) Real component

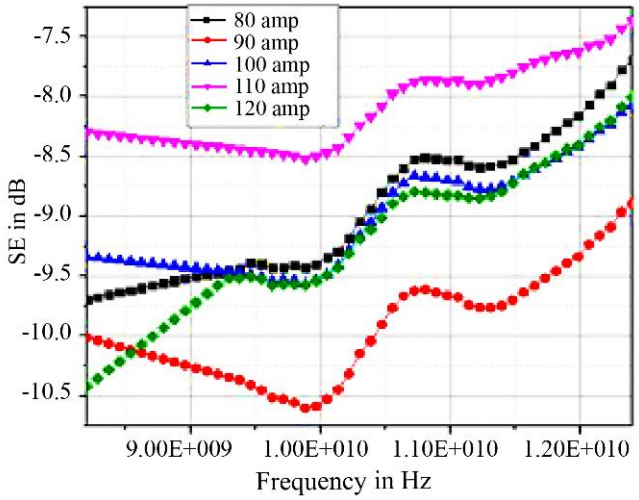

Fig. 10 Shielding effectiveness of weld joints

The real part of permeability μ′ is in the range from 1.08 to 1.23, and the imaginary part of permeability μ″ remains in the range of -0.7 to -1.1. The low permeability values of the weld joints indicate that dielectric loss significantly contributes to the weld joints' microwave absorption.

As can be seen from Fig. 9, real permeability is larger than imaginary permeability in the X-band frequency region (Real permeability = 1, Imaginary permeability = 0), and real permeability rises as weld currents rise.

The magnetic lossy filters are responsible for the increase in permeability. With increased weld current, fabricated weld joints become more effective at shielding [10]. An increase in permeability shows a significant effect on the SE of fabricated weld joints.

From fig.10, it is observed that the SE of weld joints varies in the frequency band, i.e. 8.2 GHz to 12.4 GHz. Further, all weld joints exhibit a similar trend, and the SE of all weld joints is in the range of -8.1 dB to -10.5 dB.

4. Conclusion

AA7075-T651 and AA5083-O aluminium alloys were successfully welded together with the TIG welding technique, and the following conclusions were drawn.

- Weld joints fabricated with low and high weld currents resulted in poor joint tensile strength.
- The tensile strength of a weld joint made at 100 amp current is superior to the joints made at other currents.
- Formation of intermetallics and precipitates resulted in superior joint line hardness for welds made at 120 amp current.
- Pitting corrosion characteristic of weld joints showed that the corrosion resistance of weld made at 90 amps is superior to other joints.
- EM wave properties like permeability and permeability are significantly influenced by the weld current.
- Shielding of all weld joints follows a similar trend in the entire frequency band.

References

[1] "Guidelines for Limiting Exposure to Electromagnetic Fields (100 kHz to 300 GHz)," *International Commission on Non-Ionizing Radiation Protection, Health Physics*, vol. 118, pp. 483–524, 2020. [CrossRef] [Google Scholar] [Publisher Link]

[2] M. K. Naidu et al., "Enhanced Microwave Absorption of Quartic Layered Epoxy-Mwcnt Composite for Radar Applications," *Composites and Advanced Materials*, [CrossRef] [Google Scholar] [Publisher Link]

[3] Shan Liu et al., "Lightweight High-Performance Carbon-Polymer Nanocomposites for Electromagnetic Interference Shielding," *Composites Part A: Applied Science and Manufacturing*, vol. 145, p. 106376, 2021. [CrossRef] [Google Scholar] [Publisher Link]
[4] Zhuangjun Fan et al., "Electromagnetic and Microwave Absorbing Properties of Multi-Walled Carbon Nanotubes/Polymer Composites," *Materials Science and Engineering B*, vol. 132, pp. 85–89, 2006. [CrossRef] [Google Scholar] [Publisher Link]
[5] Lee Sang-Eui, Kang Ji-Ho, and Kim Chun-Gon, "Fabrication and Design of Multi-Layered Radar Absorbing Structures of MWNT-Filled Glass/Epoxy Plain-Weave Composites," *Composite Structures*, vol. 76, pp. 397–405, 2006. [CrossRef] [Google Scholar] [Publisher Link]
[6] A Devaraju, "An Experimental Study on TIG Welded Joint between Duplex Stainless Steel and 316L Austenitic Stainless Steel," *SSRG International Journal of Mechanical Engineering*, vol. 2, no. 10, pp. 1-4, 2015. [CrossRef] [Google Scholar] [Publisher Link]
[7] Zuoyong Dou et al., "Electromagnetic Shielding Effectiveness of Aluminum Alloy-Fly Ash Composites," *Composites Part A Applied Science and Manufacturing*, vol 38, 186–191, 2007. [CrossRef] [Google Scholar] [Publisher Link]
[8] Xiangyu Ma et al., "A Novel Structure of Ferro-Aluminum Based Sandwich Composite for Magnetic and Electromagnetic Interference Shielding," *Materials and Design*, vol. 89, pp. 71–77, 2016. [CrossRef] [Google Scholar] [Publisher Link]
[9] Zuoyong Dou et al., "Electromagnetic Shielding Effectiveness of Aluminum Alloy–Fly Ash Composites," *Composites: Part A*, vol. 38, pp. 186–191, 2007. [CrossRef] [Google Scholar] [Publisher Link]
[10] Srinu Budumuru, and M. Satya Anuradha, "Electromagnetic Shielding and Mechanical Properties of AL6061 Metal Matrix Composite at X-Band for Oblique Incidence," *Advanced Composites and Hybrid Materials*, vol. 4, pp. 1113–1121, 2021. [CrossRef] [Google Scholar] [Publisher Link]
[11] Ch Hima Gireesh et al., "Study of Mechanical Properties and EMI Shielding Behavior of Al6061 Hybrid Metal Matrix Composites," *International Journal of Surface Engineering and Interdisciplinary Materials Science*, vol. 7, no. 2, pp. 48-63, 2019. [Google Scholar] [Publisher Link]
[12] Yao W Lin et al., "Effect of Silica Fume and Colloidal Graphite Additions on the EMI Shielding Effectiveness of Nickel Fiber Cement Based Composites," *Construction and Building Materials*, vol. 150, pp. 825–832, 2017. [CrossRef] [Google Scholar] [Publisher Link]
[13] Nithin Surendran et al., "Effect of TiO2 Flux and SiO2 Flux Coating on Weld Penetration by A-TIG," *SSRG International Journal of Mechanical Engineering*, vol. 5, no. 4, pp. 15-21, 2018. [CrossRef] [Google Scholar] [Publisher Link]
[14] Ying Liang et al., "Effect of TIG Current on Microstructural and Mechanical Properties of 6061-T6 Aluminium Alloy Joints by TIG-CMT Hybrid Welding," *Journal of Material Process Technology*, vol. 255, pp. 161-174, 2018. [CrossRef] [Google Scholar] [Publisher Link]
[15] A.Benoit et al., "Comparison of Four Arc Welding Processes Used for Aluminium Alloy Cladding," *Science & Technology of Welding and Joining*, vol. 20, no. 1, pp. 75-81, 2015. [CrossRef] [Google Scholar] [Publisher Link]
[16] SW Banovic, JN Dupont, and AK Marde, "Dilution and Micro Segregation in Dissimilar Metal Welds between Super Austenitic Steels and Nickel-Base Alloys," *Science and Technology of Welding and Joining*, vol. 7, no. 6, pp. 374-383, 2002. [CrossRef] [Google Schoalar] [Publisher Link]
[17] A.Kumar, and S. Sundarrajan, "Optimization of Pulsed TIG Welding Process Parameters on Mechanical Properties of AA 5456 Aluminium Alloy Weldments," *Materials & Design*, vol. 30, no. 4, pp. 1288-1297, 2009. [CrossRef] [Google Scholar] [Publisher Link]
[18] B V S R N Santhosi et al., "Comparative Study of Polymer-Based Nanocomposites Microwave Absorption Performance in X–Band," *Materials Research Express*, vol. 7, no. 1, 2020. [CrossRef] [Google Scholar] [Publisher Link]
[19] D.Mahadevi, and M.Manikandan, "Modelling and Parametric Optimization using Factorial Design Approach of Tig Welding of AZ61 Magnesium Alloy," *SSRG International Journal of Mechanical Engineering*, vol. 1, no. 1, pp. 16-20, 2014. [CrossRef] [Google Schoalar] [Publisher Link]
[20] Zuoyong Dou et al., "Electromagnetic Shielding Effectiveness of Aluminum Alloy-Fly Ash Composites," *Composites Part A, Applied Science and Manufacturing*, vol. 38, no. 1, pp. 186–191, 2007. [CrossRef] [Google Scholar] [Publisher Link]
[21] Chandrasekaran Shyamlal et al., "Corrosion Behavior of Friction Stir Welded AA8090-T87 Aluminum Alloy," *Materials*, vol. 15, vol. 15, p. 5165, 2022. [CrossRef] [Google Scholar] [Publisher Link]
[22] R.W. Fonda et al., "Microstructure, Mechanical Properties, and Corrosion of Friction Stir Welded Al 5456," *Materials Science and Engineering A*, vol. 519, pp. 1–8, 2009. [CrossRef] [Google Scholar] [Publisher Link]
[23] S. Geetha et al., "EMI Shielding: Methods and Materials—A Review," *Journal of Applied Polymer Science*, vol. 112, no. 4, pp. 2073 – 2086, 2009. [CrossRef] [Google Scholar] [Publisher Link]
[24] Mustafa Umar, and Paulraj Sathiya, "Influence of Melting Current Pulse Duration on Microstructural Features and Mechanical Properties of AA5083 Alloy Weldments," *Materials Science and Engineering A*, vol. 746, pp. 167-178, 2019. [CrossRef] [Google Scholar] [Publisher Link]
[25] Balwinder Singh, Jagjeet Singh Chatha, and Pargeet Chauhan, "Evaluation of Mechanical Properties of Friction Welded Stainless Steel Alloy 304 and Aluminium Alloy 6063 Joint," *SSRG International Journal of Mechanical Engineering*, vol. 6, no. 12, pp. 11-14, 2019. [CrossRef] [Google Scholar] [Publisher Link]
[26] G Veeraiah et al., "Influence of AC TIG Welding Current on Dissimilar AA5083 and AA7075 Aluminium Alloys," *Advances in Materials and Processing Technologies*, vol. 8, no. 4, pp. 4095-4105, 2022. [CrossRef] [Google Scholar] [Publisher Link]

[27] Waleed Ahmed W, and K. Subbaiah, "Effect of ER4047 Filler Rod on Tungsten Inert Gas Welding of AA5083-H111 and AA6061-T6 Aluminum Alloys," *Journal of Chemical and Pharmaceutical Sciences*, vol. 7, pp. 210–213, 2017. [Google Scholar]

[28] Chetan Patil, Hemant Patil, and Hiralal Patil, "Experimental Investigation of Hardness of FSW and TIG Joints of Aluminium Alloys of AA7075 and AA6061," *Frattura Ed Integrità Strutturale*, vol. 10, no. 37, pp. 325–332, 2016. [CrossRef] [Google Scholar] [Publisher Link]

[29] Avinash R. Pai et al., "Recent Progress in Electromagnetic Interference Shielding Performance of Porous Polymer Nanocomposites—A Review," *Energies*, vol. 15, no. 11, p. 3901, 2022. [CrossRef] [Google Scholar] [Publisher Link]

[30] D. Bacioiv et al., "Automated Defect Classification of Aluminium 5083 TIG Welding Using HDR Camera And Neural Networks," *Journal of Manufacturing Process*, vol. 45, pp. 603-613, 2019. [CrossRef] [Google Scholar] [Publisher Link]

[31] Jeevan Kittur et al., "A Comparative Study of EMI Shielding Effectiveness of Metals, Metal Coatings and Carbon-Based Materials," *IOP Conference Series: Materials Science and Engineering*, vol. 810, pp. 12-19, 2020. [CrossRef] [Google Scholar] [Publisher Link]

[32] Olaf Engler, and Simon Miller-Jupp, "Control of Second-Phase Particles in the Al-Mg-Mn Alloy AA 5083," *Journal of Alloys and Compounds*, vol. 689, pp. 998-1010, 2016. [CrossRef] [Google Scholar] [Publisher Link]